Available online at www.sciencedirect.com
ScienceDirect
Journal of Sound and Vibration 299 (2007) 869–883
JOURNAL OF SOUND AND VIBRATION
www.elsevier.com/locate/jsvi

Location and quantification of noise sources on a wind turbine

S. Oerlemans[a,*], P. Sijtsma[a], B. Méndez López[b]

[a]National Aerospace Laboratory NLR, P.O. Box 153, 8300 AD Emmeloord, Netherlands
[b]Gamesa Eólica, Cañada real de las merinas 7, Edificio 3, Planta 4, Madrid 28042, Spain

Received 9 September 2005; received in revised form 17 July 2006; accepted 19 July 2006
Available online 4 October 2006

Abstract

Acoustic field measurements were carried out on a three-bladed wind turbine with a rotor diameter of 58 m, in order to characterize the noise sources and to verify whether trailing edge noise from the blades was dominant. To assess the effect of blade roughness, one blade was cleaned, one blade was tripped, and one blade remained untreated. A large horizontal microphone array, positioned about one rotor diameter upwind from the turbine, was used to measure the distribution of the noise sources in the rotor plane and on the individual blades. The operation parameters of the turbine were recorded in parallel to the acoustic tests. In total more than 100 measurements were performed at wind speeds between 6 and 10 m/s. The array results reveal that besides a minor source at the rotor hub, practically all noise (emitted to the ground) is produced during the downward movement of the blades. This strongly asymmetric source pattern can be explained by convective amplification and trailing edge noise directivity. The blade noise is produced at the outer part of the blades (but not at the very tip), and the level scales with the fifth power of the local flow speed. Comparison of the noise from the individual blades shows that the tripped blade is significantly noisier than the other two. Narrowband analysis of the de-dopplerized blade noise spectra indicates that trailing edge bluntness noise is not important. All in all, the test results convincingly show that broadband trailing edge noise is the dominant noise source for this wind turbine.

1. Introduction

Wind turbine noise is one of the major hindrances for the widespread use of wind energy. In order to reduce wind turbine noise the source mechanisms must be known. For a modern large wind turbine, aerodynamic noise from the blades is generally considered to be the dominant noise source, provided that mechanical noise is adequately treated [1]. The sources of aerodynamic noise can be divided into low-frequency noise, inflow-turbulence noise, and airfoil self-noise. Low-frequency noise is caused by the aerodynamic interaction between the tower and the blades, and is considered to be of little importance for turbines with an upwind configuration (i.e. with the rotor upstream of the tower). Inflow-turbulence noise is caused by the interaction of upstream atmospheric turbulence with the leading edge of the blade, and depends on the atmospheric conditions. Airfoil self-noise is the noise produced by the blade in an undisturbed inflow, and is caused by the interaction between the turbulent boundary layer and the trailing edge of the blade. Self-noise can be tonal or broadband in character, and may be caused by several mechanisms, such as turbulent-boundary-layer-trailing-edge noise

*Corresponding author. Tel.: +31 527 248642; fax: +31 527 248210.
E-mail address: stefan@nlr.nl (S. Oerlemans).

0022-460X/$ - see front matter © 2006 Elsevier Ltd. All rights reserved.
doi:10.1016/j.jsv.2006.07.032

(subsequently denoted as trailing edge noise), trailing edge bluntness noise, or blade tip noise [1]. Both inflow-turbulence noise and airfoil self-noise can contribute to the overall sound level of a wind turbine, but the relative importance of the different mechanisms is not clear yet, and may depend on the specifications of the turbine [2].

Due to the large number of applications (e.g. wind turbines, airplanes, helicopters, fans), the characteristics of airfoil noise have been investigated extensively in both experimental and theoretical studies [3–13]. Both inflow-turbulence and self-noise mechanisms were considered and the dependence on parameters such as flow speed, angle-of-attack, radiation direction, and airfoil shape was characterized. These studies formed the basis of several semi-empirical wind turbine noise prediction models, which were validated by comparison to field measurements [14–20]. Since the field results only provided the overall sound level of the turbine, the relative importance of the different mechanisms was determined mainly on the basis of the predictions. In some studies inflow-turbulence noise was regarded to be the dominant source [11,14–16,18], while others considered trailing edge noise to be dominant [17]. In another case the turbine noise in different frequency ranges was attributed to mechanical noise, trailing edge noise, tip noise, and inflow-turbulence noise [19]. Only in a few studies source location measurements were performed to provide more direct information on the source mechanisms [21–23]. These measurements were done using an acoustic parabola or a linear microphone array, and focused only on the horizontal blade position.

The present study concerns acoustic field measurements that were carried out in the framework of the European SIROCCO project [24]. The objective of the project is to reduce wind turbine noise by designing new airfoils with low trailing edge noise emissions [25,26]. Although this concept has been successfully demonstrated for a model scale rotor [27], application to a full-scale wind turbine is only effective if trailing-edge noise is dominant. Therefore, the goal of the present field tests was to characterize the noise sources on the baseline turbine, and to verify whether trailing edge noise from the blades was dominant. The measurements were performed on a three-bladed GAMESA G58 wind turbine with a rotor diameter of 58 m. In order to assess the effect of blade roughness due to e.g. dirt or insects, before the acoustic tests one blade was cleaned, one blade was tripped, and one blade was left untreated. A large horizontal microphone array, positioned about one rotor diameter upwind from the turbine, was used to measure the distribution of the noise sources in the rotor plane and on the individual blades.

In the present paper the array results are presented and analyzed. The characteristics of mechanical and aerodynamic noise sources are investigated, and the effect of blade roughness is examined by comparing the noise from the individual blades. From these analyses the importance of the different possible source mechanisms is assessed. Section 2 describes the test set-up and the array processing methods. In Section 3 the results are presented and discussed. The conclusions of this study are summarized in Section 4.

2. Experimental method

2.1. Test set-up

The measurements were carried out on a pitch-controlled, three-bladed GAMESA G58 wind turbine, which has a rotor diameter of 58 m and a tower height of 53.5 m (Fig. 1). The turbine was located on the wind farm 'Los Monteros' in northern Spain, which has rather constant wind conditions. In order to obtain a clean inflow, a turbine on the upwind edge of the farm was chosen. About one week before the acoustic tests, one blade was cleaned, one blade was first cleaned and then tripped, and one blade remained untreated. Tripping was done using zigzag tape of 0.4 mm thickness over the complete radius, at 5% chord on the suction and pressure side of the blade. The rotor rpm was about 25, which corresponds to a tip Mach number of 0.22.

The acoustic array consisted of 148 Panasonic WM-61 microphones, mounted on a horizontal wooden platform of $15 \times 18\,m^2$. The platform was positioned about 58 m upwind from the turbine, resulting in a 'view angle' of about 45° (Fig. 2). The 'misalignment angle' α was the angle between the rotor axis (depending on wind direction) and the line from turbine to array. As a reference, two calibrated B&K microphones were placed on the platform as well. All microphones were mounted flush to the surface of the platform, with the membrane parallel to the platform, and without windscreens. The array had an elliptic shape (Fig. 3) to obtain approximately the same array resolution in the horizontal and vertical directions of the rotor plane, despite the view angle of 45°. The ellipse was slightly tilted towards the right-hand side of the rotor plane, to obtain

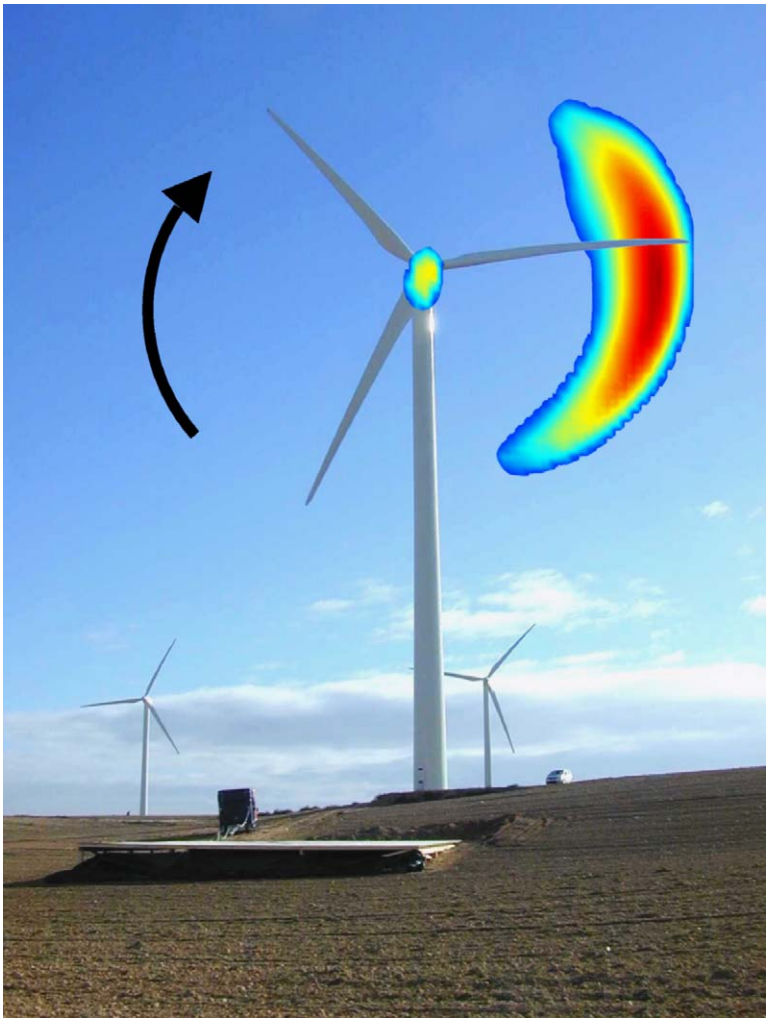

Fig. 1. Test set-up with G58 wind turbine and microphone array platform. The noise sources in the rotor plane (averaged over several revolutions) are projected on the picture.

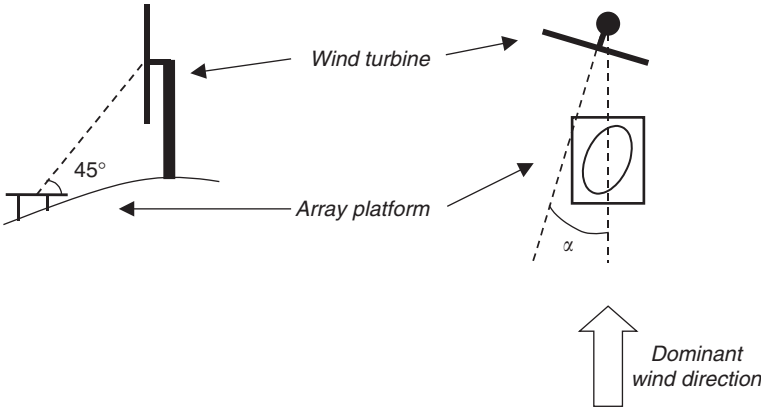

Fig. 2. Schematic picture of test set-up: side view (left) and top view (right).

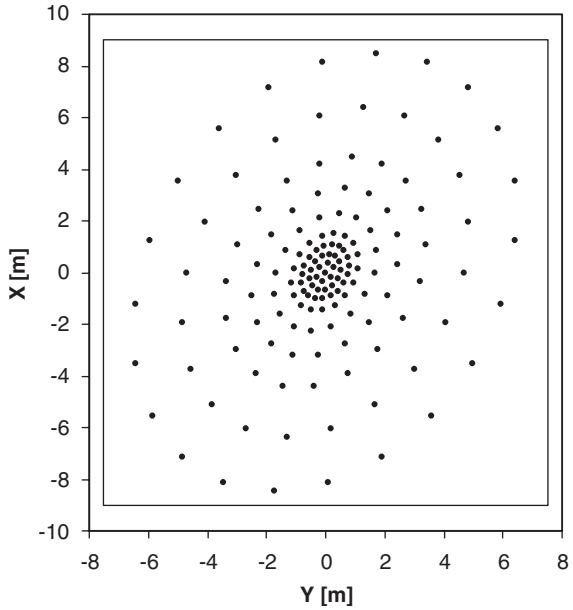

Fig. 3. Layout of array microphones. The rectangle indicates the platform dimensions.

maximum resolution on the side where the blades move downward and where maximum noise radiation was expected. The array had a high microphone density in the center to ensure low side-lobe levels at high frequencies, and a low-density outer part to obtain a good resolution at low frequencies.

2.2. Data acquisition

Acoustic data from the array microphones were synchronously measured at a sample frequency of 51.2 kHz and a measurement time of 30 s. The acoustic data were processed using a block size of 2048 with a Hanning window and an overlap of 50%, yielding 1500 averages and a narrowband frequency resolution of 25 Hz. A second-order 500 Hz high-pass filter was used to suppress high-amplitude pressure fluctuations at low frequencies, and thus extend the dynamic range to low-pressure amplitudes at high frequencies. The sound levels were corrected for the filter response and for pressure doubling due to the platform. Before the measurements, the sensitivity at 1 kHz was determined for all array microphones using a calibrated pistonphone. The frequency response of the Panasonic microphones was taken from previous calibration measurements. No corrections were applied for microphone directivity, since calibration measurements showed that these effects amounted to less than 2 dB up to 20 kHz, for angles smaller than 75° with respect to the microphone axis. Phase matching of the microphones was checked using a calibration source at known positions.

In parallel to the acoustic measurements, the following turbine operation parameters were acquired at a sample rate of 3 Hz: wind speed, power production, turbine orientation, rpm, blade pitch angle, and temperature. The measured wind speed (at the rotor hub) was translated to the wind speed at 10 m height using the standard wind profile from the IEC norm for wind turbine noise measurements [28].

2.3. Test program

During the test campaign, which lasted from 8 to 15 December 2003, a total number of 110 acoustic measurements was performed. By applying the following criteria, the 35 most stable measurements were selected for further processing:

(1) wind speed within 15% (and within 1.5 m/s) of average;
(2) misalignment angle α (see Fig. 2) smaller than 12° and within 2° of average;

Table 1
Distribution of measurements over wind speed bins

Wind speed at 10 m (m/s)	6	7	8	9	10
No. of measurements	6	6	12	5	6

(3) rotor rpm within 8% of average;
(4) blade pitch angle within 3° of average;
(5) overloads in acoustic data (e.g. due to wind gusts) less than 1%.

The above averages were calculated for the 30 s period of each acoustic measurement. The distribution of the 35 selected measurements over the different wind speed intervals is given in Table 1. It can be seen that all wind speeds are well represented. The rotor rpm typically varied between 22 and 26.

2.4. Phased array processing

The microphone array data were processed using two different methods. With the first method, noise sources in the rotor plane were localized using conventional beam forming [29]. Thus, noise from the rotor hub can be separated from blade noise, and it can be seen where in the rotor plane the blade noise is produced (see e.g. Fig. 1). The method shows the integrated effect of the three blades, averaged over the complete measurement time of 30 s (i.e. several revolutions). The first step of this processing involves the calculation of an averaged cross-spectral density matrix which contains the cross-powers of all microphone pairs in the array. To improve the resolution and to suppress background noise (e.g. wind-induced pressure fluctuations on the microphones), the main diagonal of the cross-power matrix (i.e. the auto-powers) was discarded. A frequency-dependent spatial window was applied to the microphone signals, in order to improve the resolution at low frequencies and to suppress coherence loss effects at high frequencies (due to propagation of the sound through the atmospheric boundary layer). The scan grid, with a mesh size of 1 m in both directions, was placed in the rotor plane of the wind turbine, and was rotated in accordance with the orientation of the turbine (depending on wind direction). The 6° angle between the rotor axis and the horizontal plane was also accounted for. The effect of sound convection in the atmospheric boundary layer was taken into account by assuming a constant wind speed between the scan location and the microphones. This constant wind speed was calculated as the average wind speed between the rotor hub and the array center, using the standard wind profile from the IEC norm for wind turbine noise measurements [28]. The narrowband acoustic source plots were summed to 1/3-octave bands, and the scan levels were normalized to a constant reference distance. The noise sources in the rotor plane were quantified using a source power integration method [30]. By defining one integration contour around the whole rotor plane and one only around the hub, noise levels from the hub and the blades were determined.

The second processing method used three rotating scan planes to localize the (de-dopplerized) noise sources on the three individual blades [31]. This enabled a comparison of the noise from the clean, tripped, and untreated blade. The start position of the scan planes was determined using a trigger signal from the turbine, that was recorded synchronously with the acoustic data. The mesh size of the scan grid was 0.5 m in both directions, and the scan plane was placed around the blade, in the rotor plane. Similar to the first processing method, the narrowband acoustic source plots were summed to 1/3-octave bands, and the scan levels were normalized to a constant reference distance. Since the source plots of the rotor plane indicated that practically all noise was produced during the downward movement of the blades (Fig. 1), and since the array resolution was highest on the right-hand side of the rotor plane, the blades were only scanned during their downward movement (for azimuthal angles from 0° to 180°, with 0° the upper vertical blade position). The noise from the blades was quantified using a power integration method for moving sound sources [32]. An integration contour was defined which surrounds the noise from the blade but excludes the noise from the rotor hub. In order to limit processing time, only the first two rotor revolutions after the start of each acoustic measurement were processed (one at a time). Comparison of the integrated spectra showed that the differences in average

blade noise levels between the first and second revolutions were smaller than 0.3 dB for all frequencies, which indicates a good repeatability.

3. Results and discussion

In this section the results of the acoustic array measurements are presented and analyzed. Section 3.1 describes the characteristics of the noise sources in the rotor plane, while in Section 3.2 the noise sources on the individual rotor blades are analyzed.

3.1. Noise sources in the rotor plane

In this section the distribution of the noise sources in the rotor plane is examined. The noise levels from the rotor hub and the blades are compared, and an analysis is made of convective and directivity effects. Furthermore, the speed dependence of the blade noise levels is investigated.

3.1.1. Distribution of noise sources in the rotor plane

The average source distributions in the rotor plane are shown in Fig. 4 as a function of frequency. In order to show the general trends, these source distributions were averaged over all measurements. The source plots show the integrated effect of the three blades, averaged over the complete measurement time of 30 s (i.e. several revolutions). A number of observations can be made from these plots. The most striking phenomenon is that practically all downward radiated blade noise (as measured by the array) is produced during the downward movement of the blades. Since the range of the dB scale is 12 dB, this means that the (downward radiated) noise produced during the upward movement is at least 10 dB less than during the downward movement. This effect was observed for basically all measurements and all frequencies, and is very similar to results obtained earlier on a model scale wind turbine, where it was attributed to convective amplification and directivity of trailing edge noise [27]. In Section 3.1.3 a detailed analysis will be given of this phenomenon.

A second observation in Fig. 4 is that the noise from the blades appears to dominate the noise from the rotor hub. In Section 3.1.2 the sound levels of both sources will be quantified to confirm this observation. With

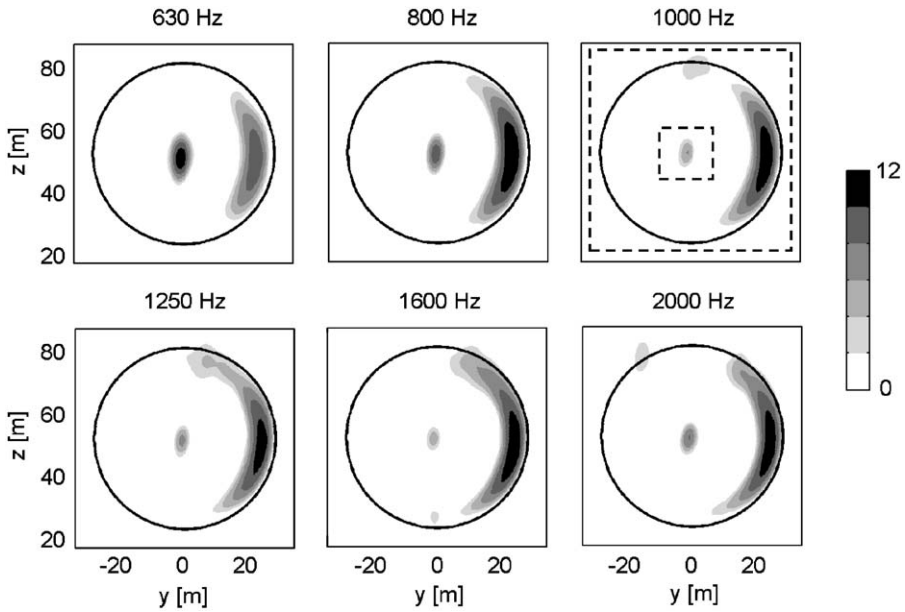

Fig. 4. Average distribution of noise sources in the rotor plane, as a function of frequency. The black circle indicates the trajectory of the blade tips. The range of the dB scale is 12 dB. The dashed rectangles at 1 kHz indicate the integration contours for the quantification of blade and hub noise.

regard to the blade noise, it can be seen that the sources are located at the outer part of the blades, but not at the very tip. Thus, tip noise is not important for the present turbine. The peak location of the blade sources moves outward for increasing frequency, from a radius of 21 m at 315 Hz to a radius of 26 m at 5 kHz. Assuming that trailing edge noise is the responsible mechanism, this can be explained by the higher flow speeds and the smaller chord at higher radii, resulting in a thinner trailing edge boundary layer. In Section 3.2.1 the source locations will be determined as a function of frequency for the individual blades. Finally, the source distributions show that blade–tower interaction effects are not significant, although at 1.6 kHz a slight noise increase is visible at the location of the tower.

3.1.2. Blade noise versus hub noise

The noise from the blades and the rotor hub was quantified using the source power integration method as mentioned in Section 2.4. The integration contours are shown in Fig. 4 (1 kHz): the small box was used for quantification of hub noise, while blade noise was defined as the difference between the integrated sound levels for the large and small boxes. The spectra in Fig. 5 (averaged over all measurements) confirm the observation from the source plots, that the blade noise is significantly higher than the noise from the hub. The hub noise shows a peak at 630 Hz, which is probably due to the gearbox. The blade noise is broadband in nature, as would be expected for trailing edge noise. The highest A-weighted levels occur around 800 Hz. Interestingly, the blade noise spectrum seems to consist of two broad 'humps': a low-frequency hump centered at 800 Hz, and a high-frequency hump starting at 2 kHz. These two humps may be caused by trailing edge noise from the suction- and pressure-side boundary layers, respectively. The difference between the overall sound pressure levels from hub and blades was found to increase with wind speed, from about 8 dB(A) at 6 m/s to about 11 dB(A) at 10 m/s. Apparently, blade noise increases faster than hub noise with increasing wind speed. In conclusion, blade noise is clearly dominant for the present wind turbine.

3.1.3. Convective amplification and directivity

Apart from a small influence from the atmospheric boundary layer and the tower, the flow conditions on the blade, and consequently the acoustic source strength, are considered to be independent of rotor azimuth. Therefore, the strong asymmetry observed in the acoustic source distributions (Fig. 4) is expected to be caused by convective (Doppler) amplification and directivity. Similar source patterns were found for a model scale wind turbine in a wind tunnel, where no wind speed gradient was present [27]. The effect of convective amplification is illustrated by the influence of the turbine orientation on the acoustic source distribution: Fig. 6 shows that the location of the source region shifts upward or downward when the right- or left-hand side of the rotor plane is turned towards the array, respectively (the misalignment angle α was defined in Fig. 2). This effect was also observed in Ref. [27], and can be qualitatively explained by the change in the component of the blade velocity in the direction of the array, which results in a change in convective amplification.

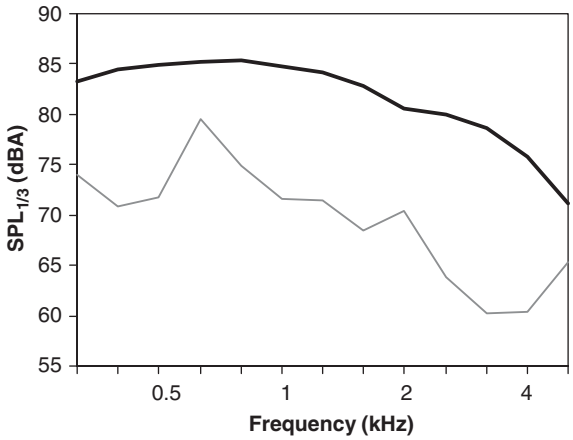

Fig. 5. Average spectra of hub noise (—) and blade noise (▬).

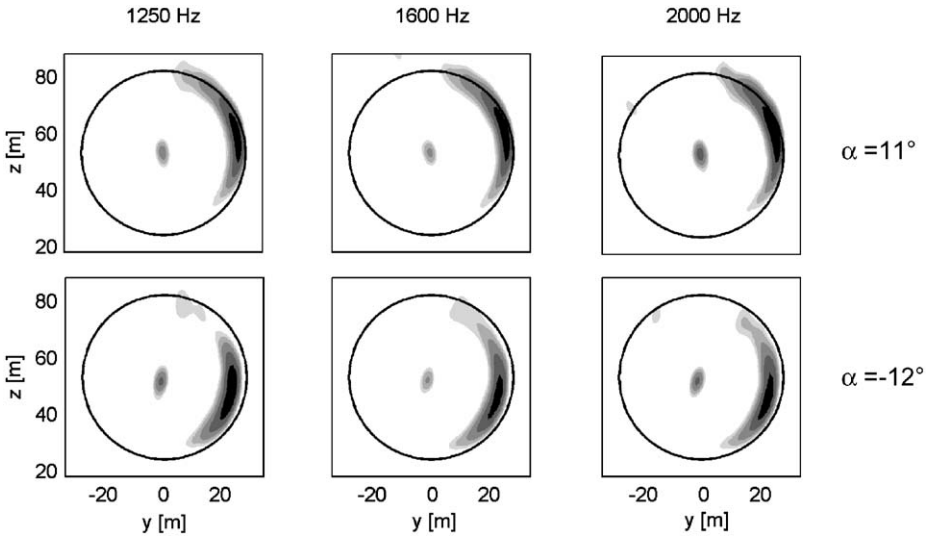

Fig. 6. Shift of blade noise location due to difference in misalignment angle α.

In order to determine if convective amplification and directivity can quantitatively explain the strong asymmetry in the measured source distribution, the expected magnitude of these effects was calculated for the present test set-up. The following directivity function for high-frequency trailing edge noise was used [33]:

$$D = \frac{2\sin^2(\theta/2)\sin^2\varphi}{(1 - M\cos\xi)^4}, \tag{1}$$

where θ is the angle between the blade chord line and the source-observer line, φ is the angle between the plane of the blade and the plane containing the chord line and the observer, ξ is the angle between the blade flow velocity and the source-observer line, and M is the (undisturbed) blade Mach number. The numerator in Eq. (1) describes the directivity of high-frequency trailing edge noise. It was analytically derived for edge noise from a semi-infinite flat plate [6,34], but was also found to be valid for finite airfoils [9], provided that the angle θ is not too close to 180° and the acoustic wavelength is smaller than the airfoil chord. Note that this directivity factor is slightly different from the factor derived by Howe [4], who used an alternative theoretical approach. In the limit for low-frequency dipole noise, where the acoustic wavelength is much larger than the airfoil chord, the $\sin^2(\theta/2)$ term changes into $\sin^2(\theta)$ [5,33]. For inflow-turbulence noise radiated from the leading edge the θ-dependence is inverted [5,11] and θ should be replaced by $(\pi-\theta)$. The denominator in Eq. (1) represents the convective amplification factor for trailing edge noise. As mentioned by Brooks and Burley [33], different exponent power laws between 1.5 and 4.5 have been found in different theoretical approaches, while experimental validation has been very limited. Following [33], here the fourth power for compact dipole sources is used [35].

For the present calculations the observer position was taken to be the center of the microphone array. The source was assumed to be located at the trailing edge of the blade at a radius of 25 m, which is the location where we typically observed blade noise (Fig. 4). In order to account for the convection of sound by the wind, so-called 'retarded' source coordinates were used [33]. For the rpm and wind speed typical values of 25 and 8 m/s were used, respectively. Fig. 7 shows the calculated convective amplification and directivity factors as a function of rotor azimuth (zero azimuth is the upper vertical blade position). It can be seen that the experimental trend is well reproduced: the calculation shows a maximum at 110° azimuth and the difference between the downward and upward blade movement is 14.9 dB. These values are in good agreement with the experimentally obtained average values of 102° azimuth and a level difference of about 15 dB between the left- and right-hand side of the rotor plane. Fig. 7 shows that the peaks for the convective amplification and directivity factors roughly coincide, and that directivity contributes most to the asymmetry. For a

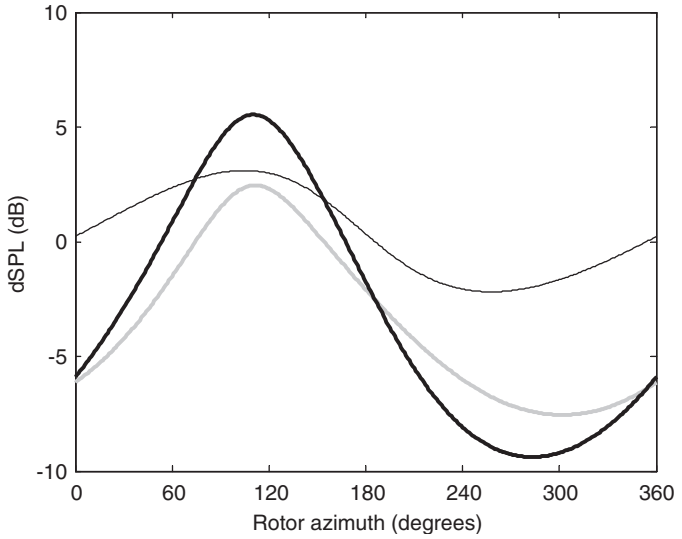

Fig. 7. Calculated convective amplification (—) and directivity (▬) factors for high-frequency trailing edge noise. The solid line (▬) indicates the combined effect.

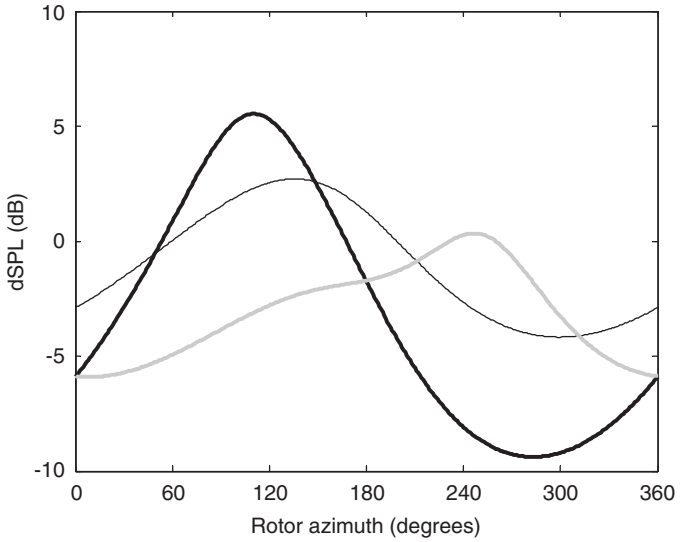

Fig. 8. Calculated combined effect of convective amplification and directivity for high-frequency trailing edge noise (▬), low-frequency dipole noise (—), and inflow-turbulence noise from the leading edge (▬).

misalignment angle of 12°, the calculated peak azimuth shifted by about 11°, in accordance with the experimental results in Fig. 6.

Since for low frequencies the acoustic wavelength is of the same order as the blade chord (0.67 m at a radius of 25 m), the directivity factor was also calculated using the low-frequency approximation with a $\sin^2(\theta)$ dependence (Fig. 8). However, these calculations show a peak azimuth of 135° and a level difference of only 6.9 dB (including the convective effect). Since the experimental results exhibited a peak azimuth around 102° and a level difference of about 15 dB for *all* frequencies (between 315 Hz and 5 kHz), the high-frequency approximation in Eq. (1) seems to be valid for the whole frequency range. Furthermore, if inflow-turbulence (leading edge) noise rather than trailing edge noise would be the responsible mechanism for the blade noise, the θ-dependence would be inverted and the peak azimuth would occur during the upward movement of the blade (Fig. 8). Thus, the present analysis shows that only the high-frequency trailing edge noise factors in

Eq. (1) satisfactorily explain the experimental results. It should be realized that the asymmetry in source locations is purely an effect of observer location, i.e. for an observer on the rotor axis the source pattern would be symmetrical. For other (far field) observer locations, Eq. (1) can be applied to estimate convective and directivity effects.

3.1.4. Speed dependence of blade noise

The speed dependence of the noise levels was investigated by calculating normalized sound levels as a function of Strouhal number $St = fL/U$, where f is frequency and L a typical length scale. For trailing edge noise, L is usually taken to be the boundary layer thickness at the trailing edge [5,6], although a recent study suggests that a constant reference length should be used [12]. Since in the present tests the trailing edge boundary layer thickness was not measured, a constant value of 1 cm was chosen for L. For U the undisturbed flow speed as perceived by the blade was used, defined as the vector sum of the wind speed and the rotational speed (induced velocity is neglected). The rotational speed was calculated for a radius of 25 m, which is the location where we typically observed blade noise (Fig. 4). The noise levels were normalized as $\mathrm{SPL}_{\mathrm{norm}} = \mathrm{SPL} - 10 \times x \times \log(U_{\mathrm{blade}}/U_{\mathrm{ref}})$, with SPL and $\mathrm{SPL}_{\mathrm{norm}}$ the measured and normalized noise levels, respectively. U_{ref} is a constant reference speed, for which here a value of 50 m/s was chosen. The variable x indicates the dependence of the blade noise on the flow speed: the acoustic energy is assumed to be proportional to the flow speed to the power of x ($p^2 \sim U^x$).

The measured and normalized blade noise spectra for the 35 individual measurements are shown in Fig. 9. The normalization was done using a value of 5 for x, which gave the best data collapse. This is indicative of trailing edge noise, since normally x is around 5 for trailing edge noise, and around 6 for inflow turbulence noise [6,10]. It can be seen that without normalization the scatter in data is 5–10 dB, even when the quietest measurement is neglected. After normalization the scatter is only 2–5 dB, including the quietest measurement. The use of a frequency-dependent source radius for the calculation of U did not significantly improve the data collapse. The remaining scatter in the normalized spectra may be due to the variation in chord and angle-of-attack along the blade radius, which leads to different trailing edge boundary layer characteristics for different source positions. Furthermore, there may be differences in turbine and weather parameters between the individual measurements. It was investigated whether the remaining scatter (after correcting for the speed effect) correlated with the misalignment angle (Fig. 2) or blade pitch angle, but no clear relation was found.

3.2. Noise sources on the individual blades

In this section the noise sources on the individual rotor blades are analyzed. Source levels and locations are compared for the clean, tripped, and untreated blade. The presence of trailing edge bluntness noise is

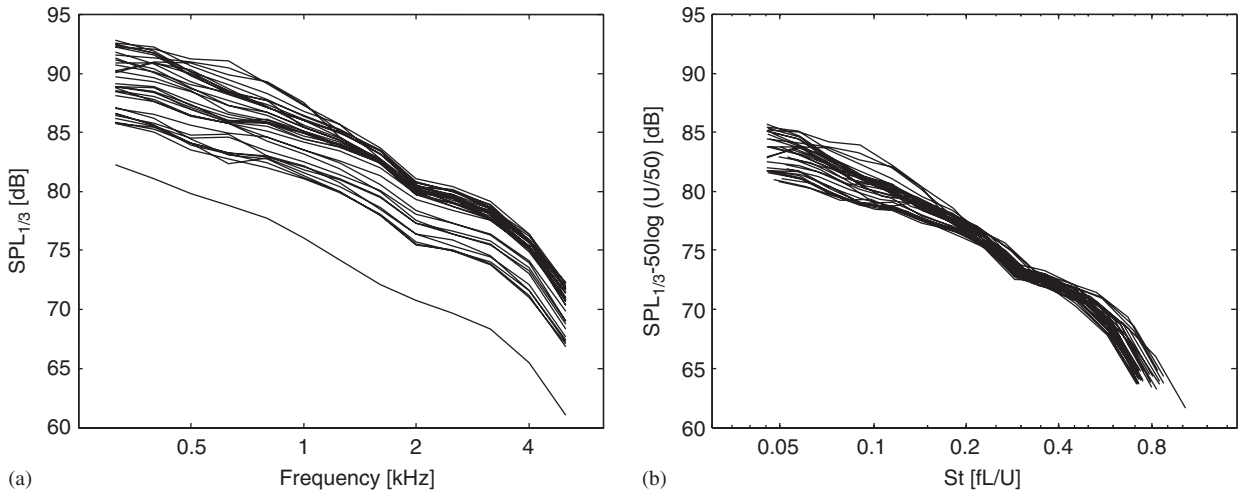

Fig. 9. Measured (a) and normalized (b) blade noise spectra for all measurements. U is the flow speed perceived by the blade.

examined by means of a narrowband analysis. Finally, the aerodynamic flow state on the untreated blade is assessed on the basis of the acoustic results.

3.2.1. Source levels and locations for the individual blades

Noise source distributions on the three individual blades, integrated over azimuthal angles from 0° to 180°, are shown in Fig. 10 for the most relevant frequency bands. The source distributions were averaged over all measurements to show the general trends. Note that the signal-to-noise ratio is very good (i.e. no spurious sources), despite the fact that only half a revolution was used (see Section 2.4). These plots confirm the observations from the source distributions in the rotor plane (Fig. 4): the blades are noisier than the hub and the relative importance of the hub is largest at 630 Hz. The aerodynamic noise is produced at the outer blades and the sources move outward with increasing frequency. In addition, Fig. 10 shows that the tripped blade is significantly noisier than the other two. This observation is a strong indication of trailing edge noise, since earlier studies have indicated that tripping does affect trailing edge noise, but has no influence on inflow turbulence (leading edge) noise [10]. Although the blade sources appear to be centered at the trailing edge, the array resolution does not seem to be sufficient to directly distinguish between leading edge and trailing edge noise. The sources for the tripped blade seem to be located at a slightly higher radius than for the clean and untreated blade.

To further investigate these observations, the source levels and locations are given in Fig. 11 for the three blades. The blade noise levels were quantified using the integration contour indicated in Fig. 10 (1 kHz). Fig. 11a clearly shows that the tripped blade is noisier than the other two for the important low frequencies, and that the tripped and untreated blades are slightly noisier than the clean blade at higher frequencies. The overall A-weighted sound level for the tripped blade was 3.6 dB(A) higher than for the clean blade, while the untreated blade was only 0.1 dB(A) noisier than the clean blade. These level differences between the blades were practically independent of wind speed. The lower peak frequency for the tripped blade can be explained by the increased boundary layer thickness at the trailing edge.

The source radius was defined as the radius at which the maximum source level occurs in the source distributions of Fig. 10. Since the mesh size of the scan grid was 0.5 m, these source radii are multiples of 0.5 m. Fig. 11b shows that, except for the highest frequencies, the sources move outward with increasing frequency, and that the source radius is largest for the tripped blade. These trends can be understood from the decrease in boundary layer thickness with increasing radius, and from the thicker boundary layer for the tripped blade. No conclusive explanation was found yet for the decrease in source radius of the tripped blade at high frequencies. This effect might be connected to noise contributions from the pressure side of the blade or to the trip thickness (0.4 mm) being relatively large for the outer blade parts (see also Section 3.2.3).

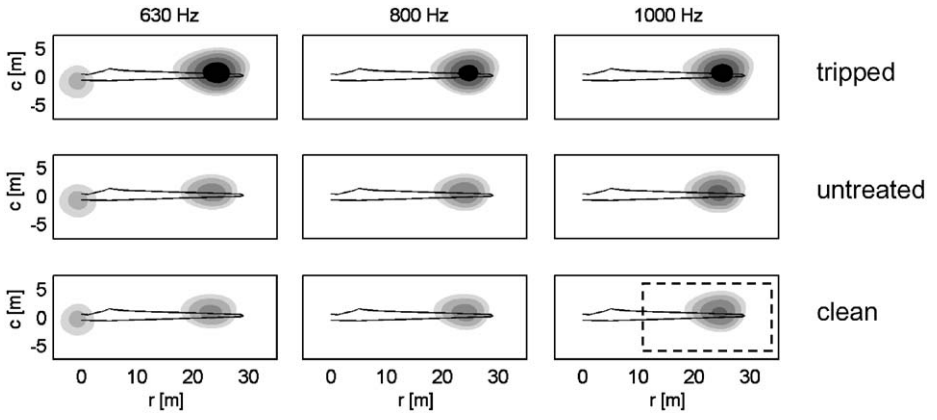

Fig. 10. Average distribution of noise sources on the individual blades. The black line indicates the blade contour (leading edge on lower side). The range of the dB scale is 12 dB and the scale is the same for the three blades. The dashed rectangle at 1 kHz indicates the integration contours for the quantification of blade noise.

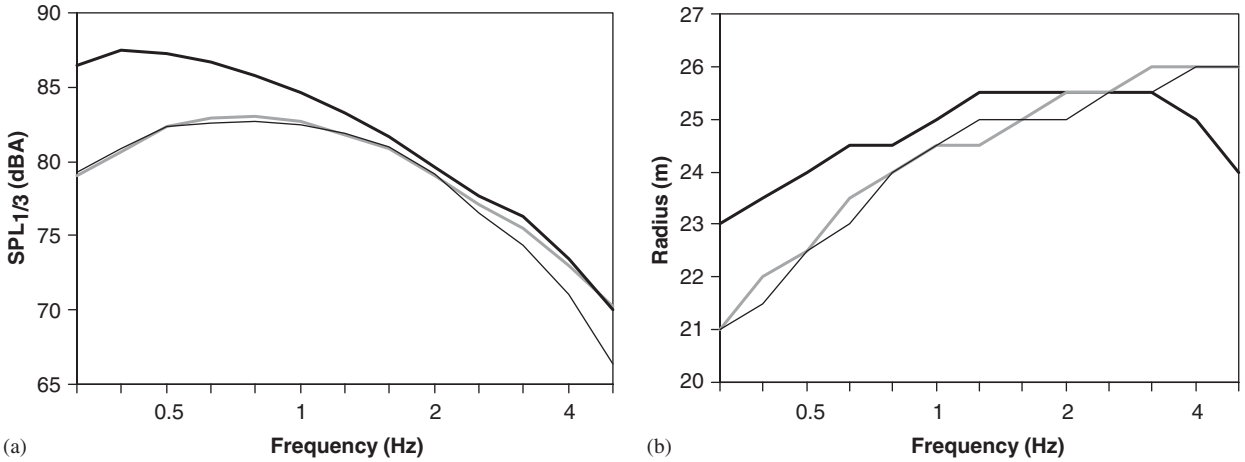

Fig. 11. Average noise source spectra (a) and source locations (b) for the three blades: ▬ tripped blade, ▬ untreated blade, — clean blade.

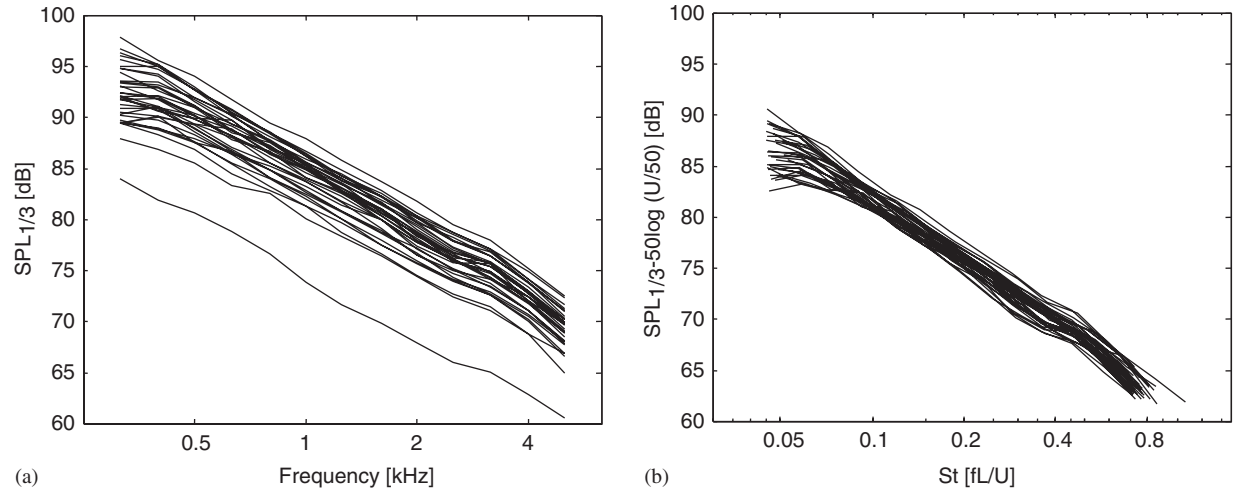

Fig. 12. Measured (a) and normalized (b) tripped blade noise spectra for all measurements. U is the flow speed perceived by the blade.

Similar to Section 3.1.4 (Fig. 9), the speed dependence of the blade noise was investigated by plotting normalized blade noise spectra as a function of Strouhal number. Again, the levels and frequencies were normalized using the flow speed at a radius of 25 m. As an example, the measured and normalized spectra for the tripped blade are shown in Fig. 12. These plots confirm that a good data collapse is obtained for $x = 5$, which is indicative of trailing edge noise. Similar to the results in Section 3.1.4, the remaining scatter in the normalized spectra may be due to the variation in chord and angle-of-attack along the blade radius, or due to differences in turbine and weather parameters between the individual measurements.

3.2.2. Trailing edge bluntness noise

When the trailing edge thickness of an airfoil is larger than about 20% of the boundary layer displacement thickness, trailing edge bluntness noise can occur [5,6,12]. Trailing edge bluntness noise is caused by periodic vortex shedding, and typically results in spectral peaks or humps, the frequency of which depends on flow speed and trailing edge (boundary layer) thickness. Bluntness noise has also been observed on wind turbines [14]. Since the blade noise spectra presented here (Fig. 12) were in 1/3-octave bands and summed over the

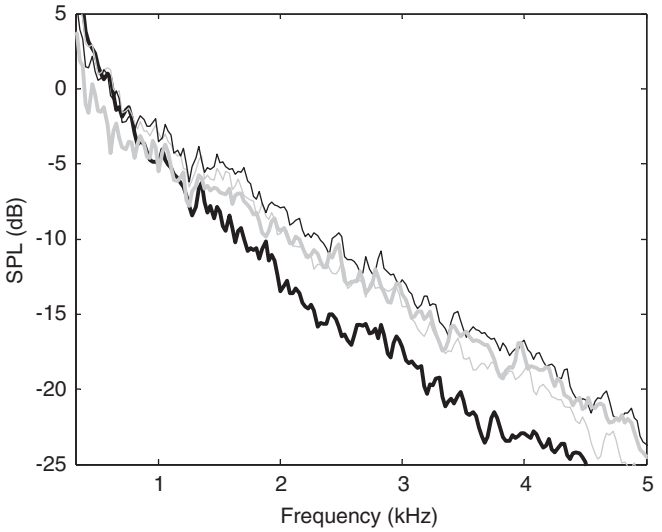

Fig. 13. Example of narrowband spectra for individual radial sections of the clean blade, illustrating absence of trailing edge bluntness noise: ▬ $r = 21$ m, —— $r = 23$ m, — $r = 25$ m, ▬ $r = 27$ m.

whole blade radius (except the hub), possible bluntness tones could be obscured. Therefore, narrowband source spectra were produced for individual radial sections, by energetically summing the chordwise scan levels in the acoustic source plots (Fig. 10) for a given radius. Fig. 13 shows an example of these radial source spectra for one measurement. Since the spectra are de-dopplerized (see Section 2.4), possible bluntness tone should have been clearly visible. However, it can be seen that only small fluctuations occur, and that no narrowband tones are identified. For the other measurements no narrowband tones were observed either, for any of the blades. Therefore, it can be concluded that trailing edge bluntness noise is not important for the present turbine.

3.2.3. Aerodynamic flow state on the rotor blades

The acoustic results can also provide information about the aerodynamic flow state on the blades, which is important input for the design of low-noise airfoils [25]. Depending on the amount of contamination, a turbine blade may be aerodynamically clean (natural boundary layer transition from laminar to turbulent) or rough (premature transition close to the leading edge). Since the flow conditions vary with blade radius, the flow state may also depend on the position on the blade. Before the present acoustic tests, it was expected that the untreated blade, which is representative for a turbine blade during normal operation, would be rough. However, the similarity between the noise levels of the clean and untreated blade (Fig. 11) suggests that the untreated blade was aerodynamically clean. An alternative explanation for this similarity could be that both the 'clean' and 'untreated' blades were in fact rough, because there was about 1 week between the cleaning of the blade and the acoustic measurements. In this case the higher levels for the tripped blade could be explained by the relatively large trip thickness (0.4 mm), which might have caused overtripping.

To get more insight in these two possibilities, two-dimensional acoustic wind tunnel tests were performed of the trailing edge noise from the GAMESA airfoil, for clean and tripped conditions [26]. These measurements showed that the trailing edge noise levels for a 0.4 mm zigzag trip (as in the field measurements) were practically identical to those for a two-dimensional turbulator strip with a thickness of 0.18 mm. This indicates that in the wind tunnel the zigzag tape did not cause overtripping. Moreover, the tripped airfoil exhibited a noise increase at low frequencies with respect to the clean airfoil, similar to the noise increase observed in the present field tests (Fig. 11). This is a strong indication that the untreated blade was aerodynamically clean during the field tests, at least for the acoustically important frequencies. The small difference between the clean and untreated blade at high frequencies may be caused by some roughness close to the tip of the untreated blade, where the boundary layer is more easily tripped and where high frequencies are produced.

4. Conclusions

Acoustic field measurements were carried out on a three-bladed wind turbine with a rotor diameter of 58 m, in order to characterize the noise sources and to verify whether trailing edge noise from the blades was dominant. To assess the effect of blade roughness, one blade was cleaned, one blade was tripped, and one blade remained untreated. A large horizontal microphone array, positioned about one rotor diameter upwind from the turbine, was used to measure the distribution of the noise sources in the rotor plane and on the individual blades.

The array results have shown that besides a minor source at the rotor hub, practically all noise (emitted to the ground) is produced during the downward movement of the blades. This strongly asymmetric source pattern was explained by convective amplification and trailing edge noise directivity. The blade noise was produced at the outer part of the blades (but not at the very tip), and the level scaled with the fifth power of the local flow speed. Comparison of the noise from the individual blades showed that the tripped blade was significantly noisier than the other two. Narrowband analysis of the de-dopplerized blade noise spectra indicated that trailing edge bluntness noise was not important. All in all, the test results have convincingly shown that broadband trailing edge noise is the dominant noise source for the present wind turbine. This conclusion is consistent with calculated results from a semi-empirical prediction code for wind turbine noise [24]. The acoustic results indicate that the untreated blade was aerodynamically clean during the field tests.

Acknowledgments

The authors would like to thank the colleagues from the University of Stuttgart and from the Netherlands Energy Research Foundation (ECN) for their valuable contributions to the definition of the tests and the interpretation of the results. The comments from A. Hirschberg (University of Twente) during the preparation of this paper are highly appreciated. Financial support for this research was given in part by the European Commission's Fifth Framework Programme, project reference: SIROCCO, Silent Rotors by Acoustic Optimisation (ENK5-CT-2002-00702). Financial support was also given by the Netherlands Organisation for Energy and the Environment (NOVEM).

References

[1] S. Wagner, R. Bareiss, G. Guidati, *Wind Turbine Noise*, Springer, Berlin, 1996.
[2] G. Guidati, J. Ostertag, S. Wagner, Prediction and reduction of wind turbine noise: an overview of research activities in Europe, American Institute of Aeronautics and Astronautics Paper 2000-0042, 2000.
[3] R. Amiet, Acoustic radiation from an airfoil in a turbulent stream, *Journal of Sound and Vibration* 41 (1975) 407–420.
[4] M.S. Howe, A review of the theory of trailing edge noise, *Journal of Sound and Vibration* 61 (1978) 437–465.
[5] W.K. Blake, *Mechanics of Flow-induced Sound and Vibration*, Academic Press, New York, 1986.
[6] T.F. Brooks, D.S. Pope, M.A. Marcolini, *Airfoil Self-noise and Prediction*, NASA Reference Publication 1218, 1989.
[7] T. Dassen, R. Parchen, G. Guidati, S. Wagner, S. Kang, A.E. Khodak, Comparison of measured and predicted airfoil self-noise with application to wind turbine noise reduction, *Proceedings of the European Wind Energy Conference*, Dublin, October 1997.
[8] G. Guidati, R. Bareiss, S. Wagner, T. Dassen, R. Parchen, Simulation and measurement of inflow-turbulence noise on airfoils, American Institute of Aeronautics and Astronautics Paper 97-1698, 1997.
[9] F.V. Hutcheson, T.F. Brooks, Effects of angle of attack and velocity on trailing edge noise, American Institute of Aeronautics and Astronautics Paper 2004-1031, 2004.
[10] S. Oerlemans, P. Migliore, Aeroacoustic wind tunnel tests of wind turbine airfoils, American Institute of Aeronautics and Astronautics Paper 2004-3042, 2004.
[11] S. Moreau, M. Roger, Competing broadband noise mechanisms in low speed axial fans, American Institute of Aeronautics and Astronautics Paper 2004-3039, 2004.
[12] M. Herr, W. Dobrzynski, Experimental investigations in low noise trailing edge design, American Institute of Aeronautics and Astronautics Paper 2004-2804, 2004.
[13] P.J. Moriarty, G. Guidati, P. Migliore, Prediction of turbulent inflow and trailing-edge noise for wind turbines, American Institute of Aeronautics and Astronautics Paper 2005-2881, 2005.
[14] F.W. Grosveld, Prediction of broadband noise from large horizontal axis wind turbine generators, American Institute of Aeronautics and Astronautics Paper 84-2357, 1984.
[15] S.A.L. Glegg, S.M. Baxter, A.G. Glendinning, *Journal of Sound and Vibration* 118 (1987) 217–239.

[16] H.H. Hubbard, K.P. Shepherd, Aeroacoustics of large wind turbines, *Journal of the Acoustical Society of America* 89 (1991) 2495–2508.
[17] M.V. Lowson, Theory and experiment for wind turbine noise, American Institute of Aeronautics and Astronautics Paper 94-0119, 1994.
[18] P. Fuglsang, H.A. Madsen, Implementation and verification of an aeroacoustic noise prediction model for wind turbines, Risø-R-867(EN), Risø National Laboratory, 1996.
[19] M.V. Lowson, J.V. Lowson, A.J. Bullmore, Wind turbine noise: analysis of results from a new measurement technique, American Institute of Aeronautics and Astronautics Paper 98-0037, 1998.
[20] P. Moriarty, P. Migliore, Semi-empirical aeroacoustic noise prediction code for wind turbines, NREL/TP-500-34478, National Renewable Energy Laboratory, Golden, CO, 2003.
[21] A. de Bruijn, W.J. Stam, W.B. de Wolf, Determination of the acoustic source power levels of wind turbines, *Proceedings of the European Wind Energy Conference*, Hamburg, October 1984.
[22] N.J.C.M van der Borg, P.W. Vink, Acoustic noise production of wind turbines in practice, *Proceedings of the European Wind Energy Conference*, Thessaloniki, October 1994.
[23] F. Hagg, G.A.M van Kuik, R. Parchen, N.J.C.M. van der Borg, Noise reduction on a 1 MW size wind turbine with a serrated trailing edge, *Proceedings of the European Wind Energy Conference*, Dublin, October 1997.
[24] J.G. Schepers, A.P.W.M. Curvers, S. Oerlemans, K. Braun, T. Lutz, A. Herrig, W. Würz, B. Méndez López, SIROCCO: SIlent rotors by acoustic optimalisation, *Proceedings of the First International Meeting on Wind Turbine Noise: Perspectives for Control*, Berlin, October 2005.
[25] T. Lutz, A. Herrig, W. Würz, K. Braun, E. Krämer, Constrained aerodynamic and aeroacoustic design of wind-rotor airfoils, *Proceedings of the First International Meeting on Wind Turbine Noise: Perspectives for Control*, Berlin, October 2005.
[26] A. Herrig, W. Würz, T. Lutz, K. Braun, E. Krämer, S. Oerlemans, Trailing-edge noise measurements of wind turbine airfoils in open and closed test section wind tunnels, *Proceedings of the First International Meeting on Wind Turbine Noise: Perspectives for Control*, Berlin, October 2005.
[27] S. Oerlemans, J.G. Schepers, G. Guidati, S. Wagner, Experimental demonstration of wind turbine noise reduction through optimized airfoil shape and trailing-edge serrations, *Proceedings of the European Wind Energy Conference 2001*, Copenhagen, 2001.
[28] IEC norm 61400-11, Wind turbine generator systems – acoustic noise measurement techniques, 2002.
[29] D.H. Johnson, D.E. Dudgeon, *Array Signal Processing*, Prentice-Hall, Englewood Cliffs, NJ, 1993.
[30] S. Oerlemans, P. Sijtsma, Acoustic array measurements of a 1:10.6 scaled airbus A340 model, American Institute of Aeronautics and Astronautics Paper 2004-2924, 2004.
[31] P. Sijtsma, S. Oerlemans, H. Holthusen, Location of rotating sources by phased array measurements, American Institute of Aeronautics and Astronautics Paper 2001-2167, 2001.
[32] P. Sijtsma, R.W. Stoker, Determination of absolute contributions of aircraft noise components using fly-over array measurements, American Institute of Aeronautics and Astronautics Paper 2004-2958, 2004.
[33] T.F. Brooks, C.L. Burley, Rotor broadband noise prediction with comparison to model data, American Institute of Aeronautics and Astronautics Paper 2001-2210, 2001.
[34] R.H. Schlinker, R.K. Amiet, Helicopter rotor trailing edge noise, NASA CR-3470, 1981.
[35] A.P. Dowling, J.E. Ffowcs Williams, *Sound and Sources of Sound*, Ellis Horwood Limited, Chichester, UK, 1983.